



HAL
open science

Assessment of the Energy Balance of Rock Masses through Discrete Element Modelling

Jabrane Hamdi, Souley Mountaka, Luc Scholtes, Marwan Al Heib, Yann
Gunzburger

► **To cite this version:**

Jabrane Hamdi, Souley Mountaka, Luc Scholtes, Marwan Al Heib, Yann Gunzburger. Assessment of the Energy Balance of Rock Masses through Discrete Element Modelling. ISRM European Rock Mechanics Symposium (EUROCK 2017), Jun 2017, Ostrava, Czech Republic. pp.442-450, 10.1016/j.proeng.2017.05.202 . ineris-01865335

HAL Id: ineris-01865335

<https://ineris.hal.science/ineris-01865335>

Submitted on 31 Aug 2018

HAL is a multi-disciplinary open access archive for the deposit and dissemination of scientific research documents, whether they are published or not. The documents may come from teaching and research institutions in France or abroad, or from public or private research centers.

L'archive ouverte pluridisciplinaire **HAL**, est destinée au dépôt et à la diffusion de documents scientifiques de niveau recherche, publiés ou non, émanant des établissements d'enseignement et de recherche français ou étrangers, des laboratoires publics ou privés.



Symposium of the International Society for Rock Mechanics

Assessment of the Energy Balance of Rock Masses through Discrete Element Modelling

Jabrane Hamdi^{a,b,*}, Mountaka Souley^a, Luc Scholtès^c, Marwan Al Heib^a,
Yann Gunzburger^b

^aINERIS, Direction des Risques du Sol et du Sous-Sol – Ecole des Mines, Campus ARTEM, CS 14234, Nancy cedex F-54042, France

^bGeoRessources – Université de Lorraine, Ecole des Mines, Campus ARTEM, CS 14234, Nancy cedex F-54042, France

^cGeoRessources – Université de Lorraine, 2 rue du Doyen Marcel Roubault, Vandoeuvre-lès – Nancy 54500, France

Abstract

With the increase of mining depth, rockbursts become one of the most serious hazards in mines. Studies of rockburst mechanisms can be done through the application of various numerical methods at the laboratory and site scales. Among the different methods available, the discrete element method (DEM) is now increasingly used thanks to its capability to explicitly model the initiation and propagation of fractures leading to failure. The paper deals with the evaluation and analysis of the energy components developing inside a rock mass by means of discrete element modeling. For this purpose, the code YADE Open DEM has been used. The rock mass is viewed as an assembly of bonded particles that interact through an elastic-brittle and frictional contact law. Interparticle breakage can occur by either tensile or shear mechanisms and interparticle friction is considered with respect to a Mohr-Coulomb criterion. Pre-existing fractures are explicitly modeled as frictional interfaces. To investigate the evolution of input and dissipated energy, various energy terms are evaluated for different loading paths. The energy terms include boundary works, elastic strain energy, friction and crack dissipation, kinetic energy and damping dissipation. The proposed energetic approach is verified by computing the energy balance of the system during simulations of compression, tension and shear tests.

© 2017 The Authors. Published by Elsevier Ltd. This is an open access article under the CC BY-NC-ND license

(<http://creativecommons.org/licenses/by-nc-nd/4.0/>).

Peer-review under responsibility of the organizing committee of EUROCK 2017

Keywords: energy balance; rock mass; discrete elements method; Yade

* Corresponding author. Tel.: +33-614-161-076.

E-mail address: jabrane.hamdi@gmail.com

1. Introduction

Rockburst is a sudden and violent phenomenon resulting from high concentration of stresses. This phenomenon is dependent on the initial and induced states of stress, on geology as well as on the presence of discontinuities in the rock mass. In damage mechanics, failure is caused by the initiation and the propagation of one or a network of microcracks. These microcracks propagate and coalesce to form fractures, leading to the rock failure. To simulate the initiation and the propagation of cracks, two approaches are generally used: the continuum and the discontinuum approach. In the continuum approach, the numerical methods are based on the finite difference (FD), finite volume (FV) and finite element (FE) methods. In this case, the initiation and propagation of cracks are modeled through the remeshing techniques which depend on the initial mesh size used. To overcome this limitation, a new numerical method has been developed: the extended finite element method (XFEM). The XFEM is able to simulate the initiation and the propagation of cracks independently of the mesh [4, 1, 2, 7]. Discrete approaches such as the discrete element method (DEM) or the discontinuous deformation analysis (DDA) provide an alternative. Cundall and Strack [3] have introduced the DEM which models the medium as an assembly of interacting particles. Each particle is identified by its mass, radius and moment of inertia and interacts with its neighbors via predefined contact laws. Potyondy and Cundall [6] then have introduced the bonded particles model (BPM) that allows simulating the behavior of rock materials and fracturing processes. Lately, the FEM/DEM has been introduced as a hybrid numerical method which combines DEM and FEM techniques. This method was initiated by Munjiza et al. [5]. In order to simulate explicitly the initiation and the propagation of cracks, we have chosen to use the computer code *Yade Open DEM* [10] where we have implemented the computation of energy terms. *Yade Open DEM* is selected because it enables us to implement the undertaken development. To validate our implementation, laboratory scale tests are simulated. In this paper, various components of energy occurring in a rock system subjected to external solicitations have been proposed. These are external work, potential energy, kinetic energy, elastic strain energy, energy dissipated by cracks, energy dissipated by numerical damping and energy dissipated by friction between particles.

Nomenclature

F_n, F_t	Normal and tangential forces
k_n, k_t	Normal and tangential stiffness
u_n, u_t	Normal and tangential displacement
c	Cohesion between particles
t	Tensile strength between particles
φ_b	Local friction angle (peak)
φ_c	Local residual friction angle
E_{el}	Elastic strain energy
E_{ki}	Kinetic energy
E_{da}	Energy dissipated by damping
E_{cr}	Energy dissipated by cracks
W_{ext}	External work
W	Energy balance
α	Damping coefficient
m	Mass of particle
v	Translational velocity of particle
I	Moment of inertia of particle
$\dot{\theta}$	Angular velocity of particle
\vec{F}	Acting force on a particle
\vec{M}	Acting moment on a particle
E_{micro}	Young modulus of particles
R_1, R_2	Radii of particle 1 and particle 2

The energy balance represents the difference between the total energy supplied to the system and that accumulated during the deformations and/or dissipated in friction and/or in cracking. Finally, this energy approach was successfully applied to numerical simulations of different laboratory tests. In this paper we limit ourselves to the calculations of the balance energy for the laboratory scale tests in order to check the robustness of the developments and to apply it in the simulation of large scale problems like underground excavation and to study rockburst phenomenon.

2. Model formulation

The simulations were performed with Yade Open DEM, a 3D code based on the DEM [10]. The rock is represented by an assembly of rigid spherical particles interacting one with each other according to an elastic-brittle contact law. The interaction force between particles is subdivided into a normal force F_n and a tangential force F_t (Fig.1). The normal force is computed such as:

$$F_n = k_n u_n \quad (1)$$

The normal stiffness is given by:

$$k_n = E_{micro} \frac{R_1 R_2}{R_1 + R_2} \quad (2)$$

And the tangential stiffness is computed via the ratio k_n/k_t which is determined by the calibration of the material.

Under compressive loading (contact closure), the normal force can increase indefinitely without overlap threshold. Under tensile loading, the normal force is limited by the maximal admissible normal force $F_{n,max}$ defined as a function of the tensile strength (t) and the surface (A_{int}) between particles:

$$F_{n,max} = t A_{int} \quad (3)$$

If $F_n \geq F_{n,max}$, tensile failure occurs and a mode I crack is created.

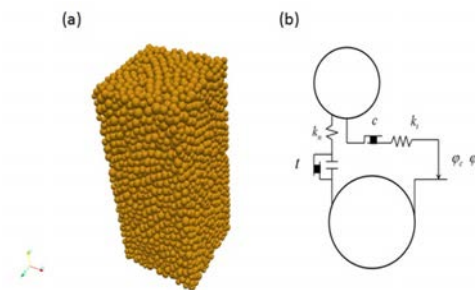


Fig. 1. (a) 3D geometrical model of a rock sample with Yade; (b) Illustration of contact between two particles.

The tangential force is calculated in an incremental manner as a function of the increment of shear displacement Δu_t that developed at the contact, such as:

$$F_t^{(t+\Delta t)} = F_t^{(t)} + k_t \Delta u_t \quad (4)$$

with $F_t^{(t+\Delta t)}$ and $F_t^{(t)}$ tangential force at the instants $t + \Delta t$ and t , respectively.

The maximal admissible shear force $F_{t,max}$ is defined as a function of the normal compression force F_n , the cohesion c , the local friction angle φ_b and the interacting surface between two particles A_{int} through a Mohr-Coulomb failure criterion:

$$F_{t,max} = F_n \tan(\varphi_b) + cA_{int} \tag{5}$$

when $F_t \geq F_{t,max}$, shear failure occurs, a mode II crack is created and the interaction between particles become purely frictional for compressive regimes or disappears for tensile regimes. For purely frictional contacts, the maximum admissible shear force is calculated as a function of and the local residual frictional angle φ_c according to:

$$F_{t,residual} = F_n \tan \varphi_c \tag{6}$$

The failure envelopes in tension and shear are illustrated in Fig. 2.

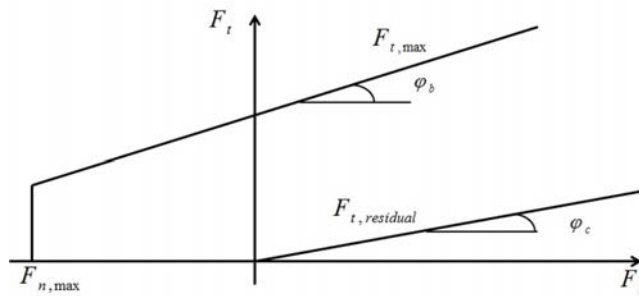


Fig. 2. Failure envelope used for the contact in Yade.

Because of the dynamic formulation of the method (explicit time domain integration), a global non-viscous damping is used to dissipate kinetic energy and facilitate convergence towards quasi-static equilibrium. This damping directly acts on the forces and torques considered in the equations of motion so that the displacements and rotations are calculated from the damped forces and damped torques such that:

$$\vec{F}_d = -\alpha \vec{F} \tag{7}$$

$$\vec{M}_d = -\alpha \vec{M} \tag{8}$$

with α the damping coefficient.

3. Energetical formulation

The DEM codes are explicit and based on the second Newton law. The different physical parameters are reachable throughout the simulation and the energetic calculation is possible. In order to calculate the balance energy with Yade, an energetic development is implemented in the code. In this development presented herein, various energy components are proposed: boundary works, elastic strain energy, friction and crack dissipation, kinetic energy and damping dissipation. These components are calculated for each time step. The increment of the elastic strain energy (ΔE_{el}) is computed as:

$$\Delta E_{el} = E_{el}^{(t+\Delta t)} - E_{el}^{(t)} = \frac{1}{2} \sum_{N_{ec}(t+\Delta t)} \left(\frac{F_n^2}{k_n} + \frac{F_t^2}{k_t} \right)^{(t+\Delta t)} - \frac{1}{2} \sum_{N_{ec}(t)} \left(\frac{F_n^2}{k_n} + \frac{F_t^2}{k_t} \right)^{(t)} \quad (9)$$

with $N_{ec}(t)$ the number of elastic contacts at time t .

The increment of the kinetic energy (ΔE_{ki}) is given by:

$$\Delta E_{ki} = \frac{1}{2} \sum_{N_p} (mv^2 + I\dot{\theta}^2)^{(t+\Delta t)} - \frac{1}{2} \sum_{N_p} (mv^2 + I\dot{\theta}^2)^{(t)} \quad (10)$$

with N_p the total number of particles, m their mass, v their translational velocity, I their moment of inertia and θ their angular velocity.

The increment of energy dissipated by damping (ΔE_{da}) is equal to:

$$\Delta E_{da} = \sum_{N_p} \alpha \left(\langle \vec{F} | \vec{v} \rangle + \langle \vec{M} | \vec{\theta} \rangle \right) \Delta t \quad (11)$$

where α is the coefficient of numerical damping, F and \vec{M} are respectively the resultant force and moment acting on the particle, Δt is the timestep, $\langle \vec{x} | \vec{y} \rangle$ is the scalar product between two vectors \vec{x} and \vec{y} .

The increment of energy dissipated during the process of cracking (ΔE_{cr}) is calculated such that:

$$\Delta E_{cr} = \frac{1}{2} \sum_{i=1}^{N_c(\Delta t)} \left(\frac{F_n^2}{k_n} + \frac{F_t^2}{k_t} \right) \quad (12)$$

where $N_c(\Delta t)$ is the number of contacts that broke during the timestep Δt .

The increment of energy dissipated by friction between particles (ΔE_{fr}) is obtained by:

$$\Delta E_{fr} = \sum_{N_{fc}} \left\langle \vec{F}_t^{(t+\Delta t)} \left| \frac{\vec{F}_t^{(t+\Delta t)} - \vec{F}_t^{(t)}}{k_t} \right. \right\rangle \quad (13)$$

where N_{fc} is the number of frictional contacts, $F_t^{(t+\Delta t)}$ and $F_t^{(t)}$ tangential force at the instants $t + \Delta t$ and t , respectively.

The increment of external work (ΔW_{ext}) is calculated such that:

$$\Delta W_{ext} = \sum_{N_w} \sum_{N_{pw}} \left\langle \vec{F}^{(t+\Delta t)} \left| \left(\vec{u}^{(t+\Delta t)} - \vec{u}^{(t)} \right) \right. \right\rangle + \sum_{N_{pb}} \left\langle \vec{F}^{(t+\Delta t)} \left| \left(\vec{u}^{(t+\Delta t)} - \vec{u}^{(t)} \right) \right. \right\rangle \quad (14)$$

where N_w is the number of walls, N_{pw} is the total number of particles for a given wall, N_{pb} is the total number of particles on the other boundaries except the walls, $\vec{F}^{(t+\Delta t)}$ is the force vector applied at instant $t + \Delta t$ and $\vec{u}^{(t)}$ and $\vec{u}^{(t+\Delta t)}$ are the displacement vector at times t et $t + \Delta t$, respectively.

The increment of the potential energy (ΔE_p) is obtained by:

$$\Delta E_p = \sum_{N_p} m \langle \vec{g} | \vec{v} \rangle \Delta t \quad (15)$$

where m mass of particle, g gravitational acceleration, \vec{v} translational velocity of particle and Δt time step.

The increment of energy balance (ΔW) is the difference between on the one hand the input energy and secondly the energy accumulated and dissipated by the system. It is given by:

$$\Delta W = \Delta W_{ext} + \Delta E_p - (\Delta E_{el} + \Delta E_{ki} + \Delta E_{da} + \Delta E_{cr} + \Delta E_{fr}) \quad (16)$$

Finally, equations (9) to (16) provide the set of energy components needed to assess the balance of a given system at each timestep Δt , and by integration the balance at each time t .

4. Applications

In order to validate the constituent equation and numerical implement, three laboratory tests are simulated: triaxial compression test, direct tension test and direct shear test. For these different tests, it is used a sample with dimensions of $1 \times 2 \times 1 \text{ m}^3$ constituted by 5000 particles calibrated on the Lac du Bonnet granite [8]. These simple configurations are chosen because analytical solutions exist or/and the results are understandable.

4.1. Triaxial compression test

A triaxial compression test with a confining pressure of 5 MPa was simulated. The test consists in two steps: hydrostatic loading with constant boundary velocity equal to 0.001 m/s until obtaining $\sigma_1 = \sigma_2 = \sigma_3 = 5 \text{ MPa}$ and deviatoric loading with axial velocity equal to 0.01 m/s. The value of the deviatoric loading velocity was chosen based on sensitivity analysis to ensure a quasi-static behavior. The different energy components were evaluated during the test as illustrated in Fig. 3 where the deviatoric stress versus axial strain has also been plotted. In the pre-peak stage, the external work and the elastic energy increase significantly with the increase of the deviatoric stress, some cracks appears in the sample and the energy is slightly dissipated by cracks and by friction between particles. In addition, the energy dissipated by damping is low. At the peak, the external work and the elastic energy reach also their maximal values. The number of cracks becomes important which results in a more and more increase of the energy dissipated by cracks, by friction between particles. In the post-peak stage, the external work slightly decreases and remains constant. The elastic energy becomes quasi-null. The number of cracks increases significantly, hence the energy dissipated by cracks increases and reaches its maximal value before remaining constant. The increase of the cracks number means the increase of the broken contacts. So the energy dissipated by friction between particles increases much because the friction between particles occurs when the contact is broken. It attains its maximum and remains constant. The energy dissipated by damping increases significantly (Fig. 3). In fact when the contact is broken the particles become free in the movement. Consequently, both damping force and moment become important in relation to the increase of translational and angular accelerations. The associated energy reaches its maximum value and remains constant. The kinetic energy E_{ki} is low in the pre-peak region. At the peak, E_{ki} attains its maximum. In the post-peak phase, the kinetic energy becomes low.

To verify the robustness of the proposed energy formulation, the balance energy ratio w^* defined as a ratio between the balance energy and the external work was computed $W^* = W/W_{ext}$. The value of this ratio varies between 1% and 3%, which validates the implementation of energy balance for triaxial compression paths (Table 1).

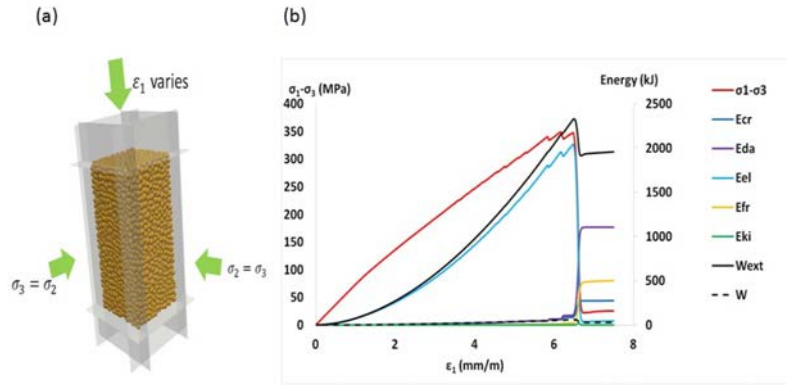


Fig. 3. (a) Geometry and boundary conditions of the triaxial compression test; (b) Evolution of the deviatoric stress and the different energy components during a triaxial compression test.

Table 1. Value of different energetic components at the end of the triaxial compression test.

Energetic components	External Work W_{ext}	Elastic Energy E_{el}	Kinetic Energy E_{ki}	Energy Dissipated by Cracks E_{cr}	Energy Dissipated by Friction E_{fr}	Energy Dissipated by Damping E_{da}	Energy Balance W	Error W^*
Value (kJ)	1956	44	0.03	275	501	1105	29	1.5%

4.2. Direct tension test

In order to calculate the energy balance for a tensile loading path, a direct tension test was simulated. The test, illustrated in Fig. 4, was run with a loading velocity equal to 0.002 m/s. This velocity was chosen by performing a sensitivity analysis to ensure a quasi-static behavior. In the pre-peak region, the external work and the elastic energy increase as the axial stress with respect to axial strain. The cracks are not created in this stage so no energy is dissipated. The kinetic energy is low in this stage. At the peak, the external work and the elastic energy reaches their maximums. In the post-peak, failure occurs, the external work becomes constant, elastic energy decreases and then remains constant. The cracks are created when failure occurs, so the energy dissipated by cracks increase. The energy dissipated by friction between particles stills low. As in triaxial compression path, the kinetic energy reaches its maximum at the peak of loading and becomes again low in the post-peak stage. The different energy components and the balance energy ratio were evaluated. It has also been noted that the values of W^* are ranged between 2% and 3%, which remains acceptable (Table 2).

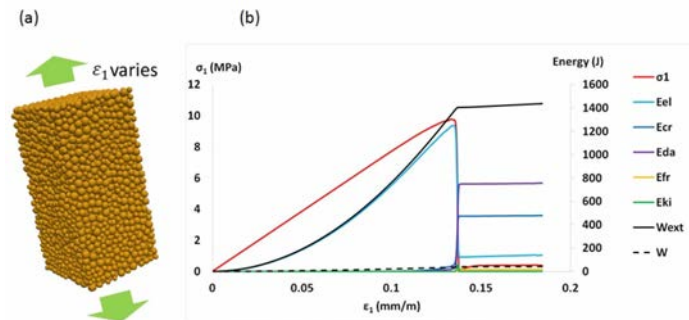


Fig. 4. (a) Illustration of direct tension test; (b) Evolution of the axial stress and the different energy components during the direct tension test.

Table 2. Value of different energetic components at the end of the direct tension test.

Energetic components	External Work W_{ext}	Elastic Energy E_{el}	Kinetic Energy E_{ki}	Energy Dissipated by Cracks E_{cr}	Energy Dissipated by Friction E_{fr}	Energy Dissipated by Damping E_{da}	Energy Balance W	Error W^*
Value (J)	1437	139	0.006	479	18	756	43	0.2%

4.3. Direct shear test

In order to evaluate the energy balance for a shear loading path, a direct shear test was simulated on a pre-fractured sample and subjected to a normal stress of 5 MPa. The test consists in two steps: applying first the normal stress until obtaining the equilibrium of the sample, and then applying the shear loading by applying the displacement velocity on the upper compartment of the shear box.

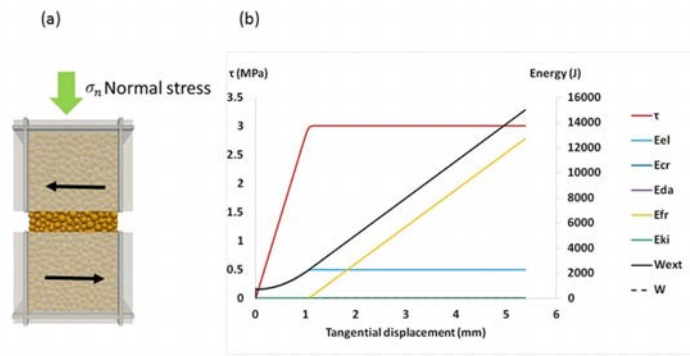


Fig. 5. (a) Illustration of the direct shear test [9]; (b) Evaluation of the shear stress and the different energy components for direct shear test.

For this test, the energy dissipated by damping and cracks are null since no cracks were created. The kinetic energy is so low during the simulation. External work, elastic energy and energy dissipated by friction between particles. In the first step of test (application of the normal stress), the external work and the elastic energy increase in the same way with the same values. Moreover the energy dissipated by friction between particles is null because the shear loading is not begun. In the second step of test (shearing process), the elastic energy becomes constant. Beyond the elastic limit, the external work and the energy dissipated by friction between particles increase with the same slope. In others words, during the sliding, the entire work of external forces is dissipated by friction. Finally, for shear loading the balance energy ratio W^* remains inferior to 0.1% (Table 3).

Table 3. Value of different energetic components at the end of the direct shear test.

Energetic components	External Work W_{ext}	Elastic Energy E_{el}	Kinetic Energy E_{ki}	Energy Dissipated by Cracks E_{cr}	Energy Dissipated by Friction E_{fr}	Energy Dissipated by Damping E_{da}	Energy Balance W	Error W^*
Value (J)	14998	2271	3.12	0	12742	25	-43	0.02%

5. Conclusion

Through this paper, it is demonstrated that the balance of energy can be correctly evaluated for different loading paths with a 3D discrete element code. The expressions of the various components of energy involved in a given system are presented as well as the way they have been implemented in the code Yade Open DEM. The quasi-null value of the energy balance W (or energy balance ration W^* less than 3%) confirm the robustness of the code regarding the energetic problems. The different energy components were correctly computed. For example, the increment of energy dissipated by friction between particles is identical to the increment of the external work during the sliding stage of the direct shear test. After the validation of the energetic developments for different loading paths, we plan to apply this energy computation to underground excavations under quasi-static and dynamic conditions with possible correlations with geophysical measurements and later to simulate the rockburst phenomenon in the underground mines.

References

- [1] Y. Abdelaziz, A. Hamouine, A survey of the extended finite element, *Computers and Structures* 86 (2008) 1141–1151.
- [2] T. Belytschko R. Gracie, G. Ventura, A review of extended/generalized finite element methods for material modeling, *Modelling and Simulation in Materials Science and Engineering* 17 (2009).
- [3] P.A. Cundall, O.D.L. Strack, A discrete numerical model for granular assemblies, *Géotechnique* 29 (1979) 47–65.
- [4] B.L. Karihaloo, Q.Z. Xiao, Modelling of stationary and growing cracks in FEM framework without remeshing: a state-of-the-art review, *Computers and Structures* 81 (2003) 119–129.
- [5] A. Munjiza, D.R.J. Owen, N. Bicanic, A combined finite-discrete element method in transient dynamics of fracturing solids, *Engineering Computations* 12 (1995) 145–174.
- [6] D.O. Potyondy, P.A. Cundall, A bonded-particle model for rock, *International Journal of Rock Mechanics & Mining Sciences* 41 (2004) 1329–1364.
- [7] C.L. Richardson, J. Hegemann, E. Sifakis, J. Hellrung, J.M. Teran, An XFEM method for modelling geometrically elaborate crack propagation in brittle materials, *International Journal for Numerical Methods in Engineering* 88 (2009) 1042–1065.
- [8] L. Scholtès, F. Donzé, A DEM model for soft and hard rocks: Role of grain interlocking on strength, *Journal of the Mechanics and Physics of Solids* 61 (2013) 352–369.
- [9] L. Scholtès, F. Donzé, Modelling progressive failure in fractured rock masses using a 3D discrete element method, *International Journal of Rock Mechanics & Mining Sciences* 52 (2012) 18–30.
- [10] V. Šmilauer, E. Catalano, B. Chareyr, S. Dorofeenko, J. Duriez, A. Gladky, J. Kozicki, C. Modenese, L. Scholtès, L. Sibille, J. Stránský, K. Thoeni, *Yade Documentation 2nd ed, The Yade Project*, DOI 10.5281/zenodo.34073 (2015).